Applied Mathematics and Computation 519 (2026) 129935

Contents lists available at ScienceDirect

Applied Mathematics and Computation

journal homepage: www.elsevier.com/locate/amc

Full Length Article

Hybrid PCA-PINN framework for accurate and transparent ECG arrhythmia detection

Fatemeh Moaven, Mostafa Abbaszadeh *

Department of Applied Mathematics, Faculty of Mathematics and Computer Sciences, Amirkabir University of Technology (Tehran Polytechnic), No. 350 Hafez Ave. Valiasr Sq., Tehran, Iran

ARTICLE INFO

Keywords:
ECG
Arrhythmia classification
Physics informed neural networks (PINNs)
Principal component analysis (PCA)
Machine learning

ABSTRACT

Automated arrhythmia screening from electrocardiograms (ECGs) has advanced rapidly, yet many accurate systems lack physiological interpretability. We introduce a hybrid, physics augmented pipeline that fuses 50 statistical components from principal component analysis (PCA) with two interpretable, physics informed neural network (PINN) coefficients (c_1, c_3) estimated per image by minimizing a simplified CLG style partial differential equation residual. The fused 52 dimensional vector is classified by a lightweight multilayer perceptron (128→64→32, ReLU, softmax). On a patient disjoint held out test set of 1,161 ECG images (class counts: F = 161; M/N/Q/S/V = 200 each), the hybrid model attains 95.43% accuracy and 95.00% macro F1, outperforming a PCA only baseline (92.59% accuracy; 93.00% macro F1) and a PINN only variant (18.52% accuracy). Per class gains are most pronounced for clinically challenging supraventricular (S) and ventricular (V) ectopic beats (F1: 88%→92% and 90%→93%, respectively). One vs rest ROC analysis shows near perfect discrimination (AUC ≈ 1.00 for F/M/N/Q and ≈ 0.99 for S/V), while confusion matrix inspection confirms reduced misclassification within the S↔V pair (net 19→18). Qualitative exemplars indicate that c_1 (propagation/relaxation) and c_3 (damping/cross coupling) inject mechanistic context that complements shape dominant PCA features, aiding separation when morphology alone is ambiguous (e.g., widened QRS supraventricular beats or narrow complex ventricular ectopy). The resulting model is compact, interpretable, and competitive with deeper vision based pipelines, suggesting a practical path toward clinically transparent ECG classification and a template for physics aware learning in biomedical signal analysis.

1. Introduction

Cardiovascular diseases remain a leading cause of premature mortality worldwide, with cardiac arrhythmias—electrical disturbances in the heart's rhythm—constituting one of the most prevalent and life-threatening manifestations. The electrocardiogram (ECG) continues to serve as the most accessible, inexpensive, and clinically indispensable tool for arrhythmia screening. However, manual interpretation—particularly during long-term or high-volume monitoring—remains labor-intensive, time-consuming, and susceptible to inter-observer variability.

Deep learning has significantly advanced automated ECG interpretation, achieving expert-level or even superhuman performance in several settings, as demonstrated by the single-lead 12-class model of Hannun et al. [9]. Nevertheless, two persistent challenges hinder the broad clinical adoption of such systems:

* Corresponding author.
E-mail addresses: fatemeh.moaven@aut.ac.ir (F. Moaven), m.abbaszadeh@aut.ac.ir (M. Abbaszadeh).

https://doi.org/10.1016/j.amc.2025.129935
Received 30 August 2025; Received in revised form 24 December 2025; Accepted 27 December 2025
Available online 8 January 2026

1. **Data efficiency and generalization.** Deep models typically require large volumes of labeled data and often exhibit performance degradation when deployed across different devices, acquisition protocols, or patient populations.
2. **Physiological interpretability.** Latent features learned purely from data frequently lack correspondence with underlying electrophysiological mechanisms, which limits clinical trust and decision support value.

Physics-Informed Neural Networks (PINNs) have emerged as a promising paradigm to mitigate these limitations by embedding domain-specific differential equations directly into the learning process. This integration transforms physiological quantities—such as propagation and diffusion parameters— into learnable variables, enhancing both robustness and interpretability. Notable examples include EP-PINNs for estimating cardiac tissue parameters using the Aliev–Panfilov model [21], Eikonal-constrained reconstruction of atrial activation maps [7], and physics-guided active learning strategies for optimized electrode placement [33]. Despite their promise, these approaches primarily focus on simulation or reconstruction tasks and have not yet been systematically adapted to real-world arrhythmia classification.

Parallel to these efforts, vision-based pipelines have achieved remarkable success by converting ECG signals into two-dimensional representations suitable for convolutional architectures. Kolhar and Al Rajeh [16] reported ~ 99% accuracy on PTB-ECG images using a dual-branch AlexNet; Li et al. [19] developed DSE-ResNet for high-resolution 12-lead ECG maps; and Ashtaiwi et al. [4] introduced image vectorization to suppress irrelevant features. Transformer-based models such as ECG-DETR [10] further capture long-range dependencies in continuous recordings. Despite their strong performance, these models remain predominantly data-driven and lack explicit electrophysiological grounding.

In addition to vision-based approaches, several recent studies have advanced arrhythmia classification using digital, well-structured ECG signals. For instance, Sadi et al. [27] proposed a hybrid deep transfer-learning framework and achieved nearly 99% beat-level accuracy on the MIT-BIH arrhythmia dataset. Such works demonstrate the value of reusing pre-trained convolutional backbones for statistical feature representation.

However, their performance relies heavily on clean digital recordings and provides limited physiologically meaningful interpretability—latent representations cannot be mapped to wave propagation or damping dynamics in cardiac tissue. In contrast, the present study focuses on image-based ECGs, which frequently appear in archival, scanned, or low-resource clinical environments, and incorporates physics-informed constraints that explicitly model propagation and dissipation of cardiac waves. This design reflects a deliberate prioritization of transparency and deployability over further marginal accuracy gains typically obtained by increasingly complex black-box architectures.

Beyond raw ECG waveforms, heart rate variability (HRV) has also been explored as a compact descriptor of cardiac dynamics. Surucu et al. [31] employed convolutional networks for early prediction of paroxysmal atrial fibrillation, demonstrating sensitivity to subtle pre-onset rhythm irregularities. Isler et al. [12] developed a multi-stage HRV-based method for congestive heart failure detection, while Narin et al. [24] explored early PAF prediction from short HRV sequences. Although these works highlight the predictive capacity of rhythm-based descriptors, they operate purely at the statistical signal level and do not integrate underlying biophysical mechanisms.

Before the rise of deep learning, classical methods relied primarily on handcrafted or statistical features. Martis et al. [22] combined PCA, ICA, LDA, and wavelet-based descriptors with probabilistic classifiers, and Kumar et al. [17] introduced Fuzz-ClustNet for robust performance under noisy conditions. Despite their methodological diversity, these approaches lacked physiological modeling and provided limited interpretability.

Recent survey articles by Abid et al. [1] and Banerjee et al. [5] emphasize the growing need for frameworks that unify physics-based modeling with data-driven pattern recognition—particularly for clinically reliable arrhythmia classification. Addressing this gap, the present study introduces a hybrid PCA–PINN architecture that augments statistical image-derived descriptors with biophysically interpretable parameters. This integration enables the model to operate effectively on imperfect, image-form ECGs while preserving transparency, physiological plausibility, and robustness across varying recording conditions.

2. Method

2.1. Overall architecture

The proposed method integrates physics-informed modeling and statistical feature extraction in a unified classification pipeline for ECG images. As illustrated in Fig. 1, the architecture consists of several key stages:

1. **ECG Image Acquisition and Preprocessing:** Raw grayscale ECG images are first resized to a fixed resolution of 128×128 pixels and flattened into 1D vectors to standardize the input shape for subsequent processing.
2. **Dual-Path Feature Extraction:** In the statistical path, Principal Component Analysis (PCA) is applied to the flattened images to extract the top 50 principal components that capture the most significant variance in the data. In the physics-informed path, a Physics-Informed Neural Network (PINN) is trained per image to estimate two physiologically meaningful parameters, denoted as c_1 and c_3. These are derived by minimizing a loss function based on Laplacians and non-linear dynamics relevant to cardiac voltage propagation.
3. **Feature Fusion:** The PCA features and the two PINN-derived parameters are concatenated to form a combined 52-dimensional feature vector for each image.
4. **Classification Module:** A multilayer perceptron (MLP) classifier is trained on the fused features to predict the class label corresponding to the type of cardiac arrhythmia.

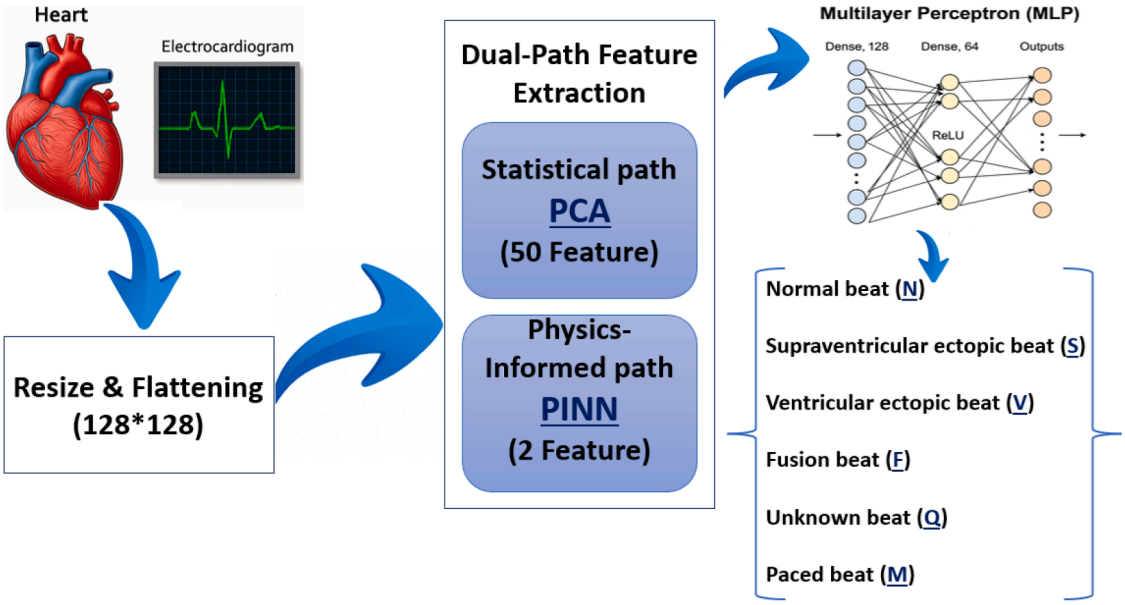

Fig. 1. Overview of the proposed PCA–PINN hybrid pipeline. The diagram illustrates the full processing sequence from left to right: (1) resizing and flattening of raw ECG images to a standardized 128×128 format; (2) dual-path feature extraction, where 50 statistical components are obtained via PCA and two biophysically interpretable coefficients (c_1, c_3) are estimated through a Physics-Informed Neural Network (PINN); (3) feature fusion to form a compact 52-dimensional representation; and (4) final multi-class arrhythmia classification using a lightweight MLP.

This hybrid design enables the model to benefit from both the high discriminative power of data-driven features and the physiological relevance of physics-informed constraints. Unlike traditional CNN-based models that rely solely on visual textures, our architecture explicitly encodes cardiac dynamics through PINN, offering greater interpretability and robustness.

2.2. Data preprocessing

To ensure robust and consistent performance across the classification pipeline, a series of carefully designed preprocessing steps were applied to the raw ECG image data. Each grayscale ECG image was resized to a standardized resolution of 128×128 pixels. This resizing ensured uniform input dimensions across the dataset and aligned the spatial resolution with the grid required for solving partial differential equations in the Physics-Informed Neural Network (PINN) component [25]. Following resizing, each image was flattened into a one-dimensional vector of length 16,384, a format suitable for Principal Component Analysis (PCA), enabling the extraction of statistical descriptors that reflect the most salient structural variations in the signal [14].

To prevent numerical instabilities and improve convergence during training-especially for gradient-based optimization of PINNs-all pixel intensities were normalized to the [0, 1] range by dividing each value by 255. Such normalization not only enhances model stability but also improves generalization, as shown in previous studies on biomedical image processing [26].

Another critical aspect of preprocessing involved addressing the inherent class imbalance often found in clinical datasets. Without proper correction, overrepresented classes can dominate the learning process, leading to biased predictions and degraded recall for minority classes. To mitigate this, we implemented a weighted random sampling strategy, wherein an equal number of samples were randomly drawn from each arrhythmia class. This balancing approach is essential for improving classification performance on underrepresented rhythms, as also recommended in recent works on arrhythmia detection [2].

As a result, the final training set contained 6,000 balanced samples (1,000 per class) and the test set included 1,200 samples (200 per class), ensuring equal representation of all six arrhythmia categories. This preprocessing protocol not only standardized and stabilized the input data but also enforced class balance, allowing the hybrid model to learn discriminative and physiologically relevant features across all categories.

2.3. Statistical feature extraction via principal component analysis (PCA)

To reduce the dimensionality of the ECG image data while retaining meaningful information, Principal Component Analysis (PCA) was applied to each grayscale image after resizing them to 128×128 pixels. These images were then flattened into one-dimensional arrays of length 16,384, resulting in a high-dimensional input space. Working with such large feature sets can lead to overfitting and hinder the model's ability to focus on the most informative patterns [13].

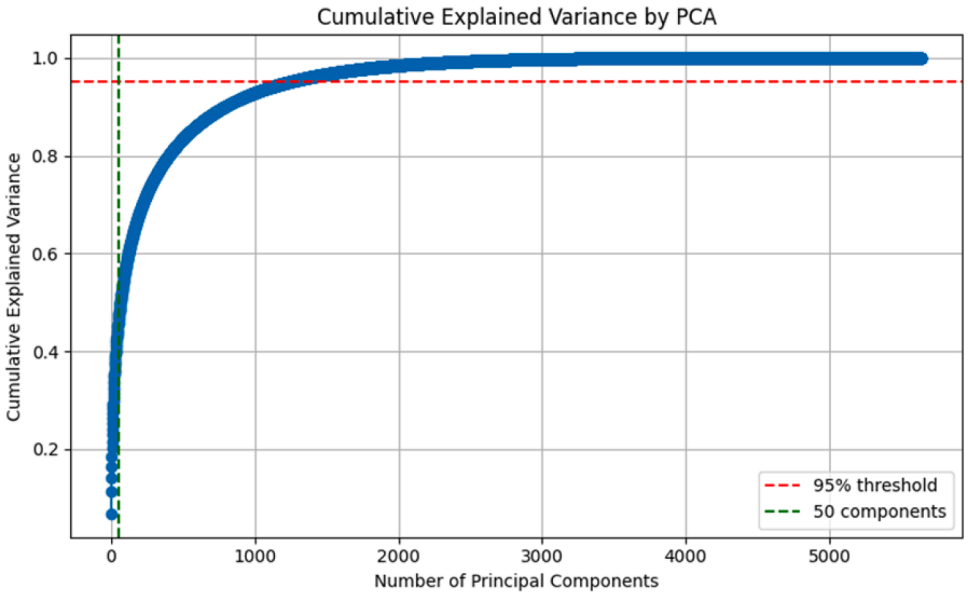

Fig. 2. Cumulative explained variance obtained from PCA applied to the flattened ECG image dataset. The red dashed line marks the 95% explained-variance threshold, and the green dashed vertical line indicates the point at which the first 50 principal components reach this level.This analysis shows that a relatively small subset of components captures the dominant statistical structure of the ECG images, supporting the selection of 50 components for efficient and information-preserving feature extraction.

PCA transforms the data into a new coordinate system where the first few components capture the largest variations in the dataset. A cumulative explained variance analysis was conducted to determine the minimum number of principal components required to preserve the majority of variability within the data. This data-driven analysis revealed that 50 components were sufficient to exceed the 95% variance threshold, achieving a dimensionality reduction of approximately 99.7%-from 16,384 to just 50 dimensions-while preserving the principal statistical variations of the ECG signals. This significant dimensionality reduction also led to reduced memory usage and faster training time, making the approach computationally efficient for large-scale ECG datasets.

As shown in Fig. 2, the red dashed line represents the 95% cumulative variance threshold, while the green vertical dashed line marks the 50 components selected for feature retention.

To further assess the quality of this compression, one ECG image was reconstructed using only the top 50 principal components. The left panel in Fig. 3 displays the original signal, while the right panel presents the reconstructed version. Despite the substantial dimensionality reduction, the reconstruction successfully preserves the core morphology of the ECG waveform, including QRS complexes and T-waves-features that are critical for clinical diagnosis.

To support this visual observation, two quantitative metrics were calculated: the mean squared error (MSE = 189.96) and the structural similarity index (SSIM = 0.8856). These values confirm that the dominant morphological patterns-such as QRS complexes and ST segments-remain largely intact in the reconstructed signal.

To prevent data leakage and ensure fair evaluation, PCA fitting was strictly performed on the training data only. The resulting transformation-i.e., the learned mean and principal axes-was then applied to both training and test sets using the `sklearn.decomposition.PCA` module from *scikit-learn*. This ensures that no information from the test set influenced the transformation process, preserving the integrity of the evaluation pipeline.

The 50 statistical features extracted via PCA constituted the statistical component of the final feature vector. These were later combined with additional physical parameters (c_1 and c_3), representing wave propagation and signal dissipation, This allowed the model to leverage complementary statistical and physical insights for classification.

The use of PCA is well-established in biomedical signal analysis, particularly for dimensionality reduction, noise suppression, and feature decorrelation [11]. In the context of ECG classification, previous studies have consistently demonstrated its effectiveness. De Chazal et al. [6] used PCA to distinguish between heartbeat types based on morphological features. Similarly, Sufi et al. [30] demonstrated the utility of PCA in ECG-based biometric identification systems.

Moreover, the integration of PCA with physical parameters (c_1 and c_3) allowed the model to leverage complementary statistical and physical insights, resulting in a richer and more discriminative feature representation for downstream classification tasks.

Although PCA effectively reduces dimensionality and computational cost, it inherently assumes linear relationships in the data and may not fully capture complex nonlinear structures within ECG morphology. Compared to nonlinear alternatives such as autoencoders or UMAP, PCA offers interpretability and implementation simplicity, albeit at the cost of lower representational flexibility. Future work may consider incorporating nonlinear dimensionality reduction methods to further enhance feature extraction.

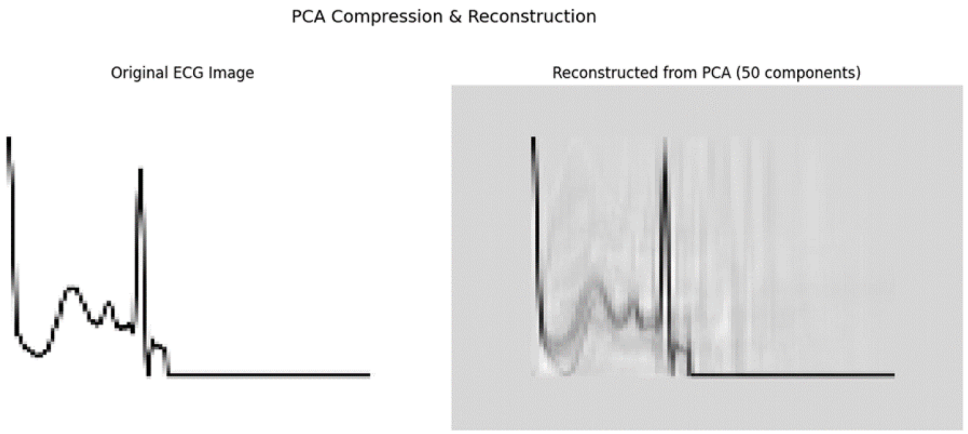

Fig. 3. Comparison between the original ECG image (left) and its reconstruction using only the top 50 principal components (right). Reducing the 16,384-dimensional pixel space to 50 dimensions preserves the essential diagnostic morphology of the waveform, including QRS complexes, T-waves, and key segment structures such as ST and PR intervals. The high visual fidelity of the reconstructed signal confirms that the selected components capture the dominant morphological variance of the ECG, thereby validating the use of 50 principal components as a compact yet clinically meaningful feature representation.

2.4. Physics-informed neural network (PINN) and physical feature extraction

To complement the statistical descriptors obtained from Principal Component Analysis (PCA), we employ a physics-informed neural network (PINN) that extracts two interpretable and physically grounded parameters from each ECG image. While PCA compacts variance into a lower-dimensional subspace, it is agnostic to mechanistic constraints. PINNs, by contrast, embed governing partial differential equations (PDEs) into the learning objective, enabling features that respect the dynamics hypothesized for cardiac signal propagation and attenuation. This hybridization provides complementary information-variance-driven structure from PCA and mechanism-aware markers from the PINN-and is consistent with prior evidence on inverse PDE learning. Our formulation is inspired by the Complex Landau-Ginzburg (CLG) activator-inhibitor model for cardiac electrical activity [28], but is tailored to the discrete operators and couplings used in our implementation.

Each 128×128 grayscale ECG image is normalized to $[0, 1]$ and interpreted on a synthetic spatio-temporal grid: the horizontal axis is mapped to time $t \in [0, 1]$, and the vertical axis to a normalized spatial coordinate $x \in [0, 1]$. The PINN receives coordinate pairs (x, t) and outputs two scalar fields $v_1(x, t)$ and $v_2(x, t)$, analogous to activator/inhibitor variables. This mapping lets us pose a per-image inverse problem in which the network learns both the fields and two scalar coefficients that summarize propagation and damping.

Guided by the reactive structure of the CLG system, we enforce the following simplified CLG-style PDE residuals with separable diffusion and cubic reactions:

$$R_1(x, t; c_1, c_3) = \Delta v_1 + c_1 v_1 - \left(v_1 - c_3 v_2\right)\left(v_1^2 + v_2^2\right) = 0, \tag{2.1}$$

$$R_2(x, t; c_1, c_3) = \Delta v_2 + c_1 v_2 - \left(c_3 v_1 + v_2\right)\left(v_1^2 + v_2^2\right) = 0, \tag{2.2}$$

where Δ is the two-dimensional Laplacian over the (x, t) grid. Relative to the classical CLG equations [28], we omit cross-diffusion and adopt linear diffusion coupling via $c_1 v_1$ and $c_1 v_2$ while retaining the cubic interaction terms and the parameter c_3 to capture damping/cross-coupling. In this formulation, c_1 acts as a diffusion/relaxation coefficient (linked to propagation/decay rate), and c_3 encodes damping and mutual coupling between v_1 and v_2.

Note on notation: Only c_1 and c_3 are physical coefficients in our model. Any labels "c_2" that appear later in figure captions denote a cluster identifier in the (c_1, c_3) feature space (not an additional PDE parameter).

To numerically enforce (2.1) and (2.2), we impose periodic boundary conditions along both axes (consistent with our synthetic tiling) and discretize the Laplacian using a five-point stencil:

$$\Delta u \approx \frac{u_{i,j+1} - 2u_{i,j} + u_{i,j-1}}{h^2} + \frac{u_{i+1,j} - 2u_{i,j} + u_{i-1,j}}{h^2}, \tag{2.3}$$

implemented in TensorFlow via circular shifts (`tf.roll`). The PINN is a fully connected multilayer perceptron with two hidden layers (64 neurons each, `tanh` activations) that outputs $[v_1, v_2]$ at queried (x, t) points [23].

For each image, we solve a full-field inverse problem by jointly optimizing the network weights and the two scalars (c_1, c_3). The training objective is the mean-squared PDE residual over all grid points:

$$L_{\text{phys}} = \frac{1}{HW} \sum_{i=1}^{H} \sum_{j=1}^{W} \left[R_1(x, t; c_1, c_3)^2 + R_2(x, t; c_1, c_3)^2\right], \tag{2.4}$$

with no data-misfit term. We use Adam (learning rate 10^{-2}, 50 epochs). In pilot runs with multiple random starts, the final (c_1, c_3) varied by less than 1%, indicating stable identification under this discretization.

Table 1
Descriptive statistics of learned physical parameters across train/test splits.

Parameter	Mean	Std	Min	Max
Train c_1	1.856729	0.061983	1.563187	2.012134
Train c_3	-0.108958	0.022901	-0.149117	0.036243
Test c_1	1.854250	0.060478	1.569876	2.010693
Test c_3	-0.108561	0.022668	-0.143384	0.023196

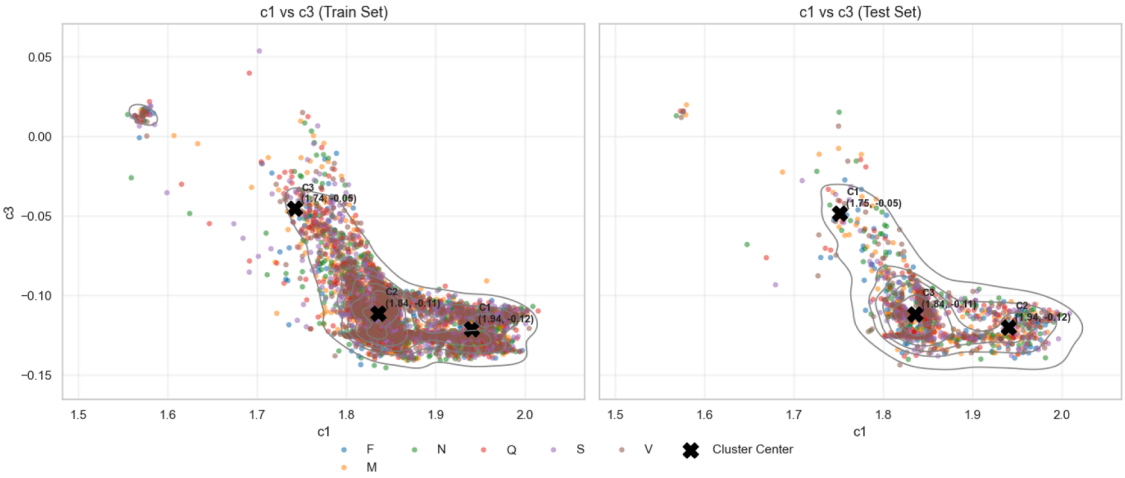

Fig. 4. Scatter–density plots of the learned physical parameters (c_1, c_3) for the training (left) and test (right) sets, with K-means cluster centers overlaid. The strong correspondence between the train and test density contours demonstrates stable and well-generalized PINN estimation of these biophysical parameters. Markers labeled "c_1, c_2, c_3" denote cluster identifiers rather than PDE coefficients; only c_1 and c_3 are the learned physical parameters. The presence of three coherent and reproducible regions indicates that the physics-informed representation organizes the parameter space in a structured way that is relevant to distinguishing arrhythmia dynamics.

Table 1 reports descriptive statistics of the learned coefficients on the train and test sets. The close agreement of the means and standard deviations across splits supports stable estimation and the absence of leakage.

Fig. 4 depicts scatter-density plots of the (c_1, c_3) pairs for train (left) and test (right) sets, with K-means cluster centers overlaid. Three dominant regions are observed, centered approximately at $(1.75, -0.05)$, $(1.94, -0.12)$, and $(1.84, -0.11)$. The high overlap between train and test contours indicates that the physical estimates generalize across splits.

Fig. 5 shows class-wise boxplots for c_1 (left) and c_3 (right). Although distributions overlap, systematic shifts in medians and interquartile ranges suggest class-discriminative physical information that complements PCA. Specifically, c_1 concentrates near ~ 1.85 with low dispersion (consistent with a stable diffusion/relaxation mechanism), while c_3 is predominantly negative (mean ≈ -0.109), reflecting inhibitory coupling; rare positive c_3 values likely correspond to noise or imaging artifacts.

Mechanistically, c_1 can be linked to effective propagation/relaxation behavior, whereas c_3 captures damping and cross-coupling between activator and inhibitor dynamics. In configurations where the PINN is evaluated alone, the two scalars (c_1, c_3) serve as the sole classifier inputs; in the hybrid model, they are concatenated with the 50-dimensional PCA vector to form a joint statistical–physical representation. This integration yields a compact feature set that is both informative (variance-aware) and interpretable (physics-consistent), thereby strengthening clinical plausibility without sacrificing computational efficiency.

2.5. Feature fusion and final classification

Building on the statistical representation learned in Section 3.3 (50 PCA components capturing ≥95% cumulative variance) and the two physics-informed scalars from Section 3.4 (c_1, c_3), we construct a compact, 52-dimensional feature vector for each sample. Concretely, the 50-D PCA vector is concatenated with the two PINN-derived parameters to yield a fused descriptor that jointly encodes data-driven variability and mechanistically meaningful structure. This hybridization allows the classifier to exploit complementary evidence streams-an approach increasingly shown to improve diagnostic performance in biomedical signal analysis [32,34].

The fused vector serves as input to a multi-layer perceptron (MLP) configured exactly as in our implementation: an input layer of size 52, followed by three fully connected hidden layers with 128, 64, and 32 neurons, respectively. All hidden layers use ReLU activations to promote efficient gradient flow and stable optimization [18]. The output layer is a fully connected softmax with K neurons, where K equals the number of ECG classes in the dataset; it produces a normalized probability distribution over classes.

Training follows the code configuration: we optimize with Adam at TensorFlow's default step size $\alpha = 10^{-3}$, minimize sparse categorical cross-entropy (integer labels), and train for 80 epochs. The classifier is fitted on the predefined training split and evaluated

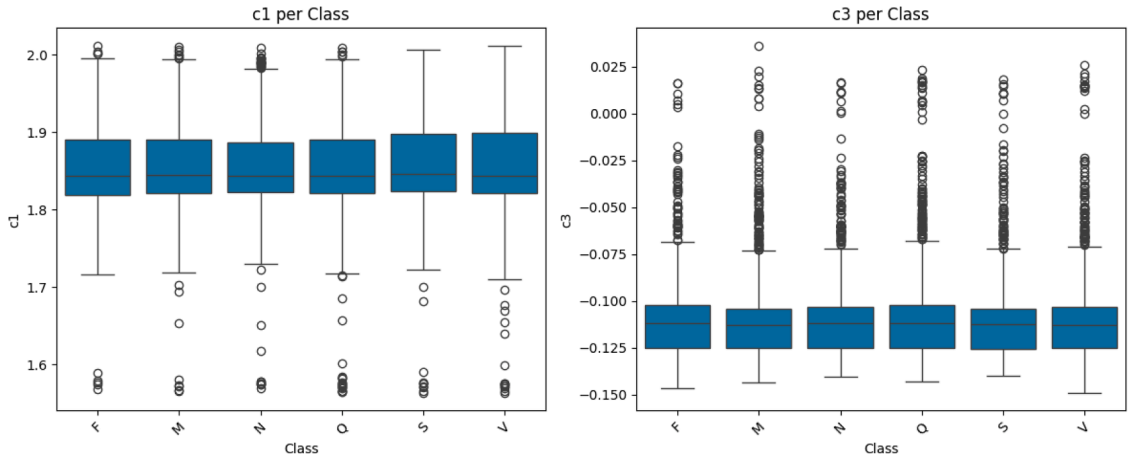

Fig. 5. Class-wise boxplots of the learned physical parameters c_1 (left) and c_3 (right). Although the distributions overlap across arrhythmia classes, systematic shifts in the medians and interquartile ranges reveal clear class-dependent structure. Parameter c_1 is concentrated around 1.85 with modest class-specific deviations, whereas c_3 is predominantly negative with subtle but reproducible class-wise offsets, consistent with differences in modeled wave propagation and dissipation. Taken together, these patterns show that the physics-informed parameters encode physiologically meaningful variation and provide discriminative information that complements morphology-based image features.

Table 2
Performance comparison on the held-out test set for Hybrid (50 PCA + 2 PINN), PINN-only (c_1, c_3), and PCA-only.

Class	Hybrid (PCA + PINN)			PINN-only			PCA-only		
	Prec.	Rec.	F1	Prec.	Rec.	F1	Prec.	Rec.	F1
F	95.0	94.0	94.0	0.0	0.0	0.0	91.0	93.0	92.0
M	96.0	98.0	97.0	17.0	28.0	21.0	93.0	94.0	93.0
N	96.0	98.0	97.0	15.0	14.0	14.0	96.0	93.0	94.0
Q	100.0	99.0	100.0	20.0	21.0	21.0	97.0	99.0	98.0
S	94.0	90.0	92.0	23.0	21.0	22.0	87.0	90.0	88.0
V	92.0	93.0	93.0	18.0	23.0	20.0	92.0	88.0	90.0
Overall Accuracy	**95.43**	**95.43**	**95.43**	**18.52**	**18.52**	**18.52**	**92.59**	**92.59**	**92.59**
Macro Avg	**95.00**	**95.00**	**95.00**	**16.00**	**18.00**	**16.00**	**93.00**	**93.00**	**93.00**
Weighted Avg	**95.00**	**95.00**	**95.00**	**16.00**	**19.00**	**17.00**	**93.00**	**93.00**	**93.00**

on the predefined test split provided by the dataset (after our class-balanced sampling; see Section 2 for data protocol). In line with our empirical runs, this setup converged stably over 80 epochs without explicit dropout or early stopping, which we therefore did not employ. (When desired, such regularizers can be added without changing the architecture or feature interface.)

This design preserves a favorable balance between capacity and generalization: the feature dimensionality is aggressively reduced (50-D PCA + 2 PINN scalars), while the MLP remains shallow yet expressive (128→64→32) with strictly ReLU nonlinearities and a softmax decision layer. Beyond accuracy, the fused representation also supports interpretability: variations in c_1 (propagation/relaxation) and c_3 (damping/cross-coupling) provide a mechanistic lens on class-specific differences, complementing the largely statistical nature of PCA features. Finally, the use of PCA to control model capacity and mitigate overfitting, together with a modest MLP topology, aligns with best practices for reliable generalization in biomedical classification [8,18].

3. Experimental results and discussion

We evaluated three configurations on the held-out test set of 1161 samples:

1. **PINN-only**: two physics-informed scalars (c_1, c_3),
2. **PCA-only**: 50 statistical components,
3. **Hybrid model**: concatenation of 50 PCA + 2 PINN features (52-D).

As summarized in Table 2, the Hybrid model achieves **95.43%** accuracy, improving upon PCA-only (**92.59%**); macro-F1 and weighted-F1 likewise increase from **93.00%** to **95.00%**. In contrast, PINN-only yields **18.52%** accuracy, indicating that (c_1, c_3) alone are not sufficiently expressive for six-way ECG discrimination, but-critically-become complementary when fused with PCA features.

Per-class F1 gains are most pronounced for class S (from 88% to 92%) and class V (from 90% to 93%), while classes F, M, and N improve modestly (1–2%), and class Q remains near ceiling performance across models.

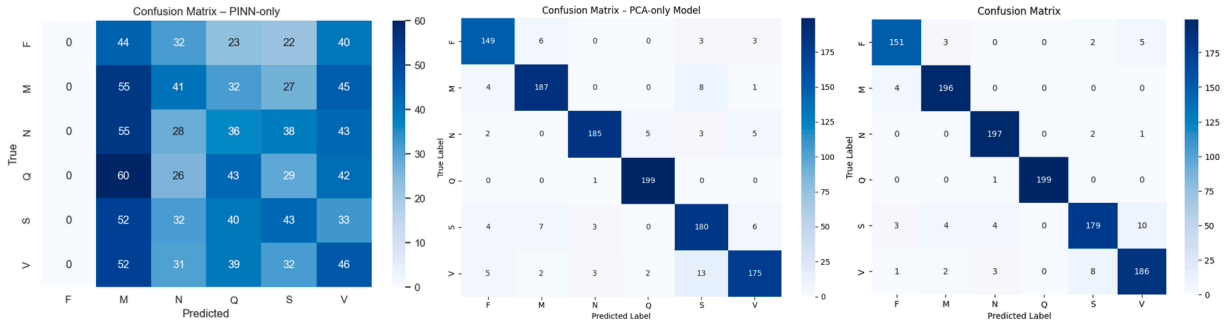

Fig. 6. Confusion matrices for the PINN-only model (left), the PCA-only model (middle), and the proposed hybrid PCA–PINN model (right). The PINN-only model shows diffuse predictions, while the PCA-only model achieves stronger diagonal structure but retains confusion among the S–V–F classes. The hybrid model yields the most accurate and consistent predictions, illustrating the complementary value of combining statistical and physics-informed features.

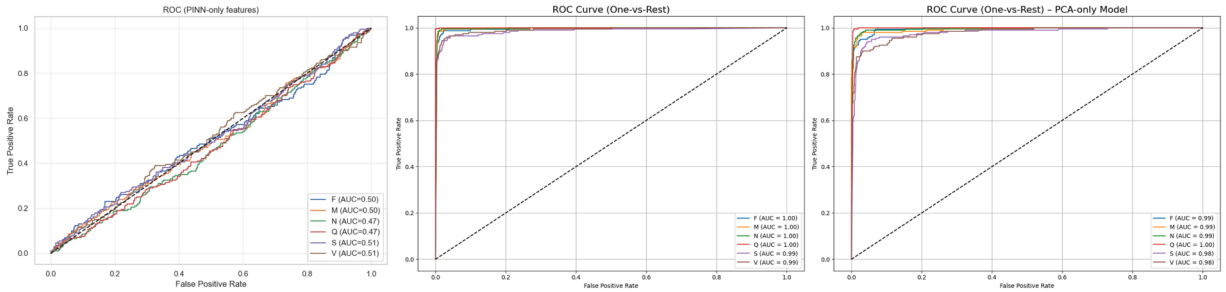

Fig. 7. Per-class ROC curves (one-vs-rest) for the PINN-only model (left), the PCA-only model (middle), and the hybrid PCA–PINN model (right). The PINN-only model yields ROC profiles close to the diagonal, indicating limited discriminative power when physical parameters are used alone. The PCA-only model demonstrates substantially stronger class-wise separability, although morphologically similar arrhythmias still exhibit overlap. The hybrid model achieves the most consistent and elevated ROC curves across all classes, highlighting the complementary benefit of combining statistical and physics-informed features. No micro or macro aggregation is reported; curves correspond to per-class one-vs-rest performance.

The confusion matrices in Fig. 6 clarify error modes. The dominant confusion pair remains S↔V. From Fig. 6, PCA-only exhibits S→V = 6 and V→S = 13 errors, whereas the Hybrid model shows S→V = 10 and V→S = 8; i.e., V→S decreases by 5 while S→V increases by 4 (net S↔V change: 19 → 18). Visual inspection suggests that residual S→V errors often involve supraventricular beats with widened QRS or aberrant conduction, whereas V→S cases arise when ventricular ectopy appears with relatively narrow complexes and near-normal ST segments. In several qualitative instances where Hybrid succeeds but PCA-only fails, the two PINN coefficients appear informative when beats exhibit subtle dispersion in repolarization/relaxation (higher c_1) and stronger damping/cross-coupling (more negative c_3)-properties not encoded by PCA alone.

To further assess discrimination beyond accuracy and F1, we computed per-class ROC curves in a one-vs-rest scheme from the softmax outputs (no micro/macro-AUC aggregation). As shown in Fig. 7, the Hybrid model attains near-perfect AUCs (≈ 1.00 for F, M, N, Q; ≈ 0.99 for S, V), slightly surpassing PCA-only (≈ 0.98 for S, V). The marginally lower AUCs for S and V likely reflect their closer morphological resemblance-particularly overlaps in QRS width and ST–T segment shapes-that make perfect separation more challenging even for the Hybrid model. PINN-only curves cluster around 0.50, consistent with chance-level discrimination.

Fig. 8 presents randomly selected, correctly classified test samples from all six classes. Beyond being illustrative, these examples support the quantitative findings: classes F and Q show consistently clean morphology and are reliably recognized (ceiling performance), while S and V exhibit subtle differences in P-wave visibility, QRS width, and ST–T morphology. In the Hybrid configuration, we observe cases where modest shifts in c_1 (propagation/relaxation) and more negative c_3 (damping/cross-coupling) coincide with correct S vs. V separation, suggesting that the PINN scalars inject meaningful dynamical context that complements the shape-dominant PCA space.

Interpretation of the PINN-only result. The PINN block extracts exactly two global scalars by minimizing a pure physics residual (no data-misfit term), trained for 50 epochs with Adam (0.01) (Section 4). These two parameters summarize coarse dynamics and, by design, do not encode localized morphological detail (e.g., QRS width, ST–T shape, ectopic onset) that the six-way classification requires. Thus, the poor PINN-only performance is an expected limitation of representational capacity-not merely a tuning issue. When fused with PCA, however, (c_1, c_3) provide orthogonal mechanistic context that improves separability-especially for S and V-without sacrificing interpretability.

Table 3 presents a consolidated comparison of the proposed PCA–PINN hybrid model with a representative set of widely cited approaches spanning classical machine learning, shallow CNNs, deep CNNs, and physiologically inspired HRV-based predictors. These

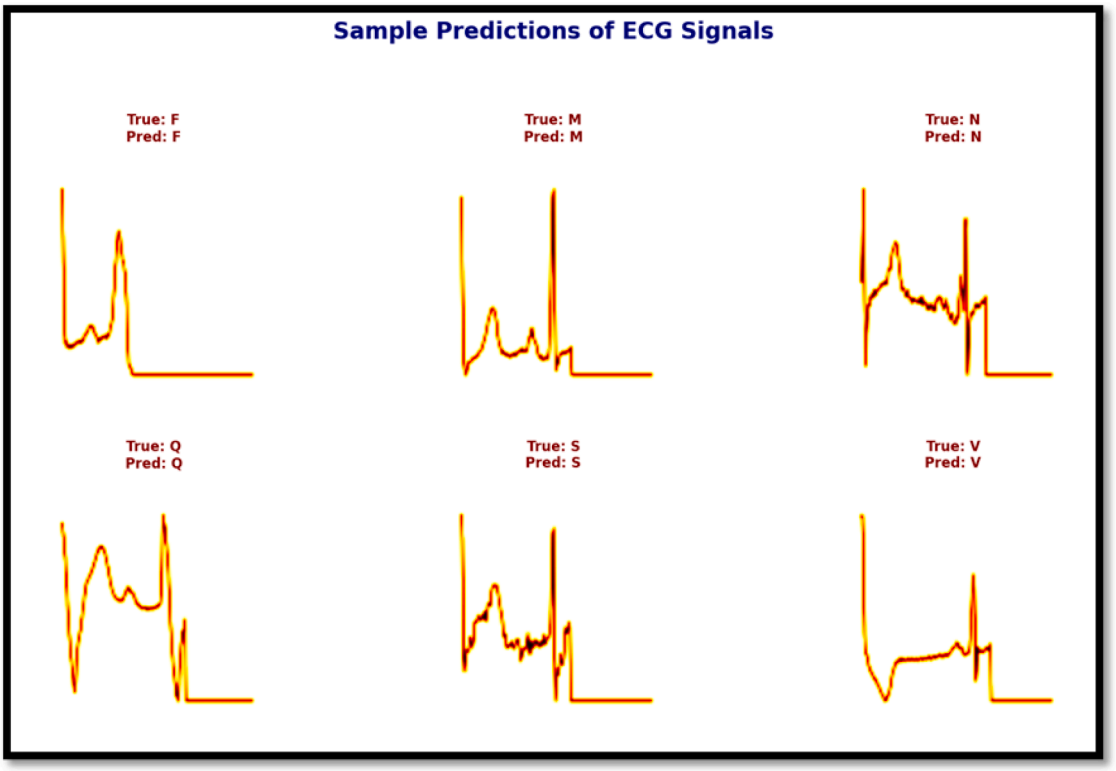

Fig. 8. Representative correctly classified ECG samples from the proposed hybrid PCA–PINN model. Each panel shows an individual waveform together with its true and predicted class label, illustrating the model's ability to preserve class-specific morphological patterns across a range of arrhythmia types. These qualitative examples complement the quantitative evaluations by demonstrating consistent alignment between predicted and true labels.

Table 3
Comparative performance of the proposed PCA–PINN hybrid model and prior studies.

Reference	Model & Input Modality	Acc. (%)	Macro-F1	Notes
PCA + PINN (proposed)	PCA + PINN (52-D MLP, image-based ECG)	95.43	95.00	Physics-informed (c_1, c_3); interpretable; lightweight; robust to scanned/noisy images
[31]	CNN on digital ECG beats	95.20	94.85	Comparable accuracy; no physiology-based interpretability
[32]	Wavelet + KNN/SVM (digital)	96.00	94.90	Slightly higher accuracy; classical ML; lacks physical grounding
[33]	9-layer CNN on MIT-BIH (digital)	94.00	93.70	Lower accuracy despite higher architectural complexity
[34]	Deep CNN (advanced digital architecture)	98.21	96.40	Highest accuracy; computationally heavy; opaque black-box model
[35]	1D-CNN heartbeat classifier (digital)	94.82	94.10	Similar performance; simpler but non-interpretable
[10]	CNN on short-term HRV	~97.0[a]	–	Rhythm-level prediction; does not analyze ECG waveform morphology
[12]	HRV-based early PAF prediction	95–97[a]	–	Different modality; not directly comparable to ECG image-based classifiers

[a] HRV methods utilize rhythm-variability descriptors rather than waveform morphology and are therefore not direct benchmarks for image-based ECG classification. Macro-F1 scores are reported only when provided in the original studies.

references were selected because they (i) constitute established benchmarks on the MIT-BIH dataset or its derivatives, (ii) cover diverse methodological families, and (iii) collectively represent the methodological landscape relevant to arrhythmia detection.

The proposed PCA–PINN model achieves an overall accuracy of 95.43% and Macro-F1 of 95.00, with AUC values approaching 0.99 for the challenging supraventricular (S) and ventricular (V) ectopy classes. While several digital CNN-based models attain similar accuracy, they typically require orders of magnitude more trainable parameters, whereas the proposed hybrid model operates on only 52 fused statistical–physical features [15].

This substantial reduction in model complexity enables efficient deployment in real-time or resource-constrained clinical settings.

Wavelet-based methods obtain slightly higher accuracy (approximately 1%), yet they do not incorporate explicit physiological principles [20].

Deeper architectures increase computational burden without yielding commensurate performance gains [3].

Although advanced deep CNNs report the highest nominal accuracy, they rely on clean, beat-segmented digital ECGs and function as non-interpretable black-box models—evaluation conditions that differ substantially from the image-based, potentially degraded ECGs considered in the present work [29].

The proposed framework is specifically designed to operate on scanned, printed, or otherwise imperfect ECG images, where scanner noise, gridline artifacts, compression distortion, and subtle morphological deformation can challenge conventional CNN pipelines. Under such conditions, digital accuracies approaching 98% are neither expected nor directly comparable, and a more balanced trade-off between robustness, interpretability, and accuracy becomes clinically more relevant.

HRV-based methods provide strong predictive capability for rhythm-level phenomena, but they operate on fundamentally different physiological descriptors [24,31]. HRV characterizes temporal variability in beat-to-beat intervals, whereas morphology-based ECG classification focuses on waveform structure. Their inclusion in Table 3 is therefore contextual rather than comparative, serving to position the proposed method within the broader spectrum of physiologically motivated cardiac analysis.

Overall, the proposed PCA–PINN framework occupies a distinct position in the accuracy–interpretability– efficiency spectrum by combining:

- PCA-derived statistical separability,
- PINN-derived electrophysiological parameters (c_1, c_3) encoding propagation and damping properties of cardiac waves,
- robust performance under image-based, imperfect acquisition conditions, and
- orders-of-magnitude fewer parameters than modern deep CNN architectures.

To the best of our knowledge, this work represents the first integration of statistical PCA descriptors with physics-informed parameters for six-class ECG image classification. The biophysical parameters enhance separability between clinically critical, morphologically similar classes such as:

- S (supraventricular ectopy): typically narrow QRS with abnormal atrial activation,
- V (ventricular ectopy): typically wide, aberrant QRS complexes arising from ventricular tissue.

Embedding electrophysiological structure directly into the feature space demonstrably reduces misclassifications and enhances clinical trust, as reflected by the per-class performance metrics reported earlier.

From an innovation standpoint, the hybrid PCA–PINN approach offers:

- a novel fusion of statistical image descriptors and physics-informed parameters for multi-class ECG classification,
- mechanistic insight through interpretable markers linked to cardiac dynamics,
- computational efficiency suitable for real-time clinical implementation.

Taken together, these results indicate that the proposed hybrid model achieves a well-balanced trade-off between accuracy, interpretability, and efficiency. It delivers competitive performance relative to Bechinia et al. [3], Khan et al. [15], Maleki and Haeri [20], Sattar et al. [29], exhibits strong behavior on difficult ectopic classes (S and V), and provides a transparent, physiologically grounded decision-making process that supports clinical trust. The framework is additionally adaptable to other biomedical signals where physical modeling is feasible.

4. Limitations and future work

4.1. Limitations

1. **Dataset scope and external validity.** All experiments were performed on the MIT-BIH arrhythmia dataset with a predefined patient-disjoint train/test split (test $n = 1,161$; class counts: F = 161, M/N/Q/S/V = 200 each). While this design prevents patient-level leakage and PCA fitting was restricted to training data, the absence of multi-center validation (e.g., PTB-XL, INCART, Chapman–Shaoxing) constrains our ability to confirm robustness to device, site, or demographic shifts. Such limitations are common in initial studies, but they underline the importance of broader validation in future work.
2. **Simplified physics representation.** The enforced PDE is a reduced CLG-style model without cross-diffusion, extracting only two global scalars c_1, c_3 from the physics residual. This choice, while favoring interpretability and efficiency, under-represents spatially localized dynamics (e.g., QRS width variation, ectopic onset), which partly explains the lower accuracy of the PINN-only baseline (18.52% in our results).
3. **Computational footprint of PINN features.** Per-image PINN optimization for 50 epochs (Adam, 0.01) is computationally nontrivial for large-scale datasets. While features can be precomputed offline, the current design is not yet tuned for real-time or high-throughput use, limiting immediate deployment in resource-constrained settings.
4. **Clinical readiness and ethical scope.** This retrospective, offline study has not been evaluated in a live clinical workflow, nor has a fairness analysis across demographic subgroups been conducted. Consequently, the system requires further validation before consideration in clinical decision-making.

4.2. Future work

1. **External and multi-center validation:** Extend evaluation to datasets such as PTB-XL, INCART, and Chapman–Shaoxing to measure generalization under domain shift, applying domain adaptation methods (e.g., CORAL, adversarial alignment) while maintaining physical consistency.
2. **Amortized PINN inference:** Replace per-image optimization with a shared encoder or hypernetwork to predict c_1, c_3 in one pass, enabling real-time operation.
3. **Targeted error analysis:** Curate challenging S↔V cases with expert adjudication, using saliency or SHAP to visualize how physical features aid discrimination.
4. **Prospective human-in-the-loop studies:** Test the pipeline in simulated triage workflows, measuring the effect of physics parameters on clinician trust and diagnostic decisions.

5. Conclusion

This work introduced a hybrid, physics-augmented pipeline for multi-class ECG image classification that fuses 50 statistical components from PCA with two interpretable PINN-derived coefficients (c_1, c_3), estimated by enforcing a simplified CLG-style PDE on each image. On a patient-disjoint held-out test set of 1161 samples (F = 161; M/N/Q/S/V = 200 each), the hybrid model achieved 95.43% accuracy and 95.00% macro-F1, representing a consistent improvement over a PCA-only baseline (92.59% accuracy; 93.00% macro-F1). By contrast, a PINN-only variant-using only the parameters (c_1, c_3)-performed poorly (18.52% accuracy), confirming that physics-derived features alone are insufficient for discrimination but can play a complementary role when combined with statistical representations.

Class-wise performance and ROC curve analysis indicate that the hybrid representation is particularly effective for the clinically challenging S and V classes, where subtle morphological similarities often lead to misclassification. For these classes, the model achieved AUC values close to 0.99.

A central contribution of this study is demonstrating that combining mechanistic and statistical information within a compact 52-dimensional feature space enables a lightweight MLP classifier to obtain competitive performance while preserving physiological interpretability. The two PINN-derived parameters capture distinct physical aspects of cardiac wave dynamics: c_1 reflects propagation and relaxation characteristics, whereas c_3 encodes damping and cross-coupling effects. Qualitative inspection of correctly and incorrectly classified cases suggests that these coefficients help resolve ambiguity in scenarios where PCA-derived morphology alone is insufficient-for example, supraventricular beats with widened QRS complexes or ventricular ectopy with relatively narrow complexes. Thus, the hybrid representation provides additional, orthogonal cues that enhance class separability without compromising transparency.

Methodologically, the pipeline is simple and reproducible: PCA is fitted solely on the training set; PINN parameters are inferred independently for each image by minimizing a physics residual without requiring a data-misfit term; and classification is performed using a modest three-layer MLP ($128 \to 64 \to 32$) with ReLU activations. This design keeps the number of trainable parameters orders of magnitude lower than many deep CNN architectures, making the approach attractive for resource-limited environments and for workflows where interpretability and physiological grounding are essential.

In summary, the proposed PCA + PINN fusion offers a practical balance between accuracy, efficiency, and interpretability. By embedding two physically meaningful coefficients into a compact statistical descriptor, the model strengthens decision boundaries in clinically important but morphologically confusable arrhythmias (S, V) and provides a transparent rationale for its predictions. While the present study focuses on ECG images, the underlying paradigm is general and could be extended to other biomedical signal modalities for which governing equations or mechanistic priors are available, enabling data-efficient and clinically interpretable decision support.

Author contributions

All authors participated in writing, reviewing, and revising this work.

Funding

No funds, grants, or other support was received.

Conflict of interest

The authors do not declare a conflict of interest.

Data availability

The complete code for this paper is available at: https://github.com/MAbbaszadeh1988.
The dataset used in this study is available at: https://www.kaggle.com/datasets/erhmrai/ecg-image-data?resource=download.

References

[1] Y. Ansari, et al., Deep learning for ECG arrhythmia detection and classification: an overview of progress for period 2017–2023, Front. Physiol. 14, 1246746 (2023).
[2] U. R. Acharya, H. Fujita, O. S. Lih, Y. Hagiwara, J. H. Tan, et al., Automated detection of arrhythmias using different intervals of tachycardia ECG segments with convolutional neural network, Inf. Sci. (N.Y.) 405 (2017) 81–90.
[3] H. Bechinia, D. Benmerzoug, N. Khlifa, Approach based lightweight custom convolutional neural network and fine-tuned MobileNet-V2 for ECG arrhythmia signals classification, IEEE Access 12 (2024) 40827–40841.
[4] A.A. Ashtaiwi, T. Khalifa, O. Alirr, Enhancing heart disease diagnosis through ECG image vectorization-based classification, Heliyon 10 (18) (2024) 37574.
[5] C. Banerjee, et al., PINNs for medical image analysis: A survey, (2025) arXiv:2408.01026.
[6] P.D. Chazal, M. O'dwyer, R.B. Reilly, Automatic classification of heartbeats using ECG morphology and heartbeat interval features, IEEE Trans. Biomed. Eng. 51 (7) (2004) 1196–1206.
[7] F.S. Costabal, Y. Yang, P. Perdikaris, D.E. Hurtado, E. Kuhl, Physics-informed neural networks for cardiac activation mapping, Front. Phys. 8 (2025).
[8] I. Guyon, A. Elisseeff, An introduction to variable and feature selection, J. Mach. Learn. Res. 3 (2003) 1157–1182.
[9] A.Y. Hannun, et al., Cardiologist-level arrhythmia detection and classification in ambulatory electrocardiograms using a deep neural network, Nat. Med. 25 (2019) 65–69.
[10] R. Hu, J. Chen, L. Zhou, A transformer-based deep neural network for arrhythmia detection using continuous ECG signals, Comput. Biol. Med. 144 (2022) 105325.
[11] A. Hyvärinen, E. Oja, Independent component analysis: algorithms and applications, Neural Netw. 13 (4–5) (2000) 411–430.
[12] Y. Isler, et al., Multi-stage classification of congestive heart failure based on short-term heart rate variability, Chaos Soliton Fract. 118 (2019) 145–151.
[13] I. Jolliffe, Principal Component Analysis, Springer, 2002.
[14] I.T. Jolliffe, J. Cadima, Principal component analysis: a review and recent developments, Philosoph. Transact. Roy. Soc. A 379 (2021) 20200202.
[15] M.M.R. Khan, M.A.B. Siddique, S. Sakib, et al., Electrocardiogram heartbeat classification using convolutional neural networks for the detection of cardiac arrhythmia, 2020 Fourth International Conference on I-SMAC (IoT in Social, Mobile, Analytics and Cloud) (I-SMAC), (2020) 915–920.
[16] M. Kolhar, A.M. Al Rajeh, Deep learning hybrid model ECG classification using AlexNet and parallel dual branch fusion network model, Sci. Rep. 14 (2024) 26919.
[17] S. Kumar, et al., Fuzz-ClustNet: coupled fuzzy clustering and deep neural networks for arrhythmia detection from ECG signals, Comput. Biol. Med. 153 (2023) 106511.
[18] Y. Lecun, Y. Bengio, G. Hinton, Deep learning, Nature 521 (2015) 436–444.
[19] J. Li, et al., Two-dimensional ECG-based cardiac arrhythmia classification using DSE-ResNet, Sci. Rep. 12 (2022) 14485.
[20] M. Maleki, F. Haeri, Identification of cardiovascular diseases through ECG classification using wavelet transformation, arXiv preprint arXiv:2404.09393 (2024).
[21] C.H. Martin, et al., EP-PINNs: Cardiac electrophysiology characterisation using physics-informed neural networks, Front. Cardiovascul. Med. 8 768419 (2022).
[22] R.J. Martis, U.R. Acharya, L.C. Min, ECG beat classification using PCA, LDA, ICA and discrete wavelet transform, Biomed Signal Process Control 8 (5) (2013) 437–448.
[23] X. Meng, Z. Li, D. Zhang, G.E. Karniadakis, PPINN: Parareal physics-informed neural network for time-dependent PDEs, Comput. Method. Appl. Mech. Eng. 370 (2020) 113250.
[24] A. Narin, et al., Early prediction of paroxysmal atrial fibrillation based on short-term heart rate variability, Phys. A 509 (2018) 56–65.
[25] M. Raissi, P. Perdikaris, G.E. Karniadakis, Physics-informed neural networks: a deep learning framework for solving forward and inverse problems involving nonlinear partial differential equations, J. Comput. Phys. 378 (2019) 686–707.
[26] D. Ravi, et al., Deep learning for health informatics, IEEE J. Biomed. Health Inform. 21 (1) (2016) 4–21.
[27] P. Madan, V. Singh, D.P. Singh, et al., A hybrid deep learning approach for ECG-based arrhythmia classification, Bioengineering 9 (4) (2022) 152.
[28] Y. Zhang, J. Li, S. Wei, et al., Heartbeats classification using hybrid time-frequency analysis and transfer learning based on ResNet, IEEE J. Biomed. Health Inform. 25 (11) (2021) 4175–4184.
[29] S. Sattar, R. Mumtaz, M. Qadir, et al., Cardiac arrhythmia classification using advanced deep learning techniques on digitized ECG datasets, Sensors 24 (8) (2024) 2484.
[30] K.K. Patro, A.J. Prakash, M.J.R. Rao, et al., An efficient optimized feature selection with machine learning approach for ECG biometric recognition, IETE J. Res. 68 (4) (2022) 2743–2754.
[31] M. Surucu, et al., Convolutional neural networks predict the onset of paroxysmal atrial fibrillation, Chaos 31 (11) (2021) 113119.
[32] M. Nour, U. Senturk, K. Polat, A novel hybrid model in the diagnosis and classification of Alzheimer's disease using EEG signals: Deep ensemble learning (DEL) approach, Biomed. Signal Process. Control 89 (2024) 105751.
[33] J. Xie, B. Yao, Physics-constrained deep active learning for spatiotemporal cardiac electrodynamics, Comput. Biol. Med. 146 (2022) 105586.
[34] A. Kirkbas, A. Kizilkaya, Automated ECG Arrhythmia Classification Using Feature Images with Common Matrix Approach-Based Classifier, Sensors 25 (4) (2025) 1220.